Feasibility of Retrieving Land-Surface Temperature From ASTER TIR Bands Using Two-Channel Algorithms: A Case Study of Agricultural Areas

Juan C. Jiménez-Muñoz and José A. Sobrino

***Abstract*—The Advanced Spaceborne Thermal Emission and Reflection Radiometer (ASTER) provides the user community with standard products of land-surface temperature (LST) and emissivity using the temperature and emissivity separation (TES) algorithm. This letter analyzes the feasibility of using two-channel (TC) algorithms for LST retrieval from ASTER data, which could be considered as an alternative or complementary procedure to the TES algorithm. TC algorithms have been developed for all the ASTER thermal infrared bands combinations, and they have been applied to six ASTER images acquired over an agricultural area of Spain in 2000, 2001, and 2004. LST values obtained with TC algorithms were compared with the TES product. In addition, the TC algorithms were tested using simulated data and ground-based measurements collected coincident with the ASTER acquisition in 2004. The results show that TC algorithms provide similar accuracies than the TES algorithm (∼1.5 K), with the main advantage that the atmospheric correction is included in the algorithm itself.**

***Index Terms*—Advanced spaceborne thermal-emission and reflection radiometer (ASTER), land-surface temperature (LST), split window (SW), temperature and emissivity separation (TES), thermal infrared (TIR), two channel (TC).**

I. Introduction

THE ADVANCED Spaceborne Thermal Emission and Reflection Radiometer (ASTER) is a high spatial resolution 14-band multispectral imager on the Terra satellite, which was launched in December 1999 as part of the National Aeronautics and Space Administration's (NASA) Earth Observing System. ASTER provides observations in three spectral regions using three separate radiometers: bands 1–3 covering the visible and-near-infrared region 0.52–0.86 μm at 15-m resolution; bands 4–9 covering the short wavelength infrared region 1.60–2.45 μm at 30-m resolution; and bands 10–14 covering the thermal infrared (TIR) region 8–12 μm at 90-m resolution. The five ASTER TIR bands from 10 to 14, discussed in this letter, have spectral ranges of 8.125–8.475, 8.475–8.825, 8.925–9.275, 10.25–10.95, and 10.95–11.65 μm, with effective wavelengths of 8.279, 8.635, 9.074, 10.659, and 11.267 μm, respectively. The radiometric accuracy for the TIR bands is specified to be ± 3 K at 200–240 K, ± 2 K at 240–270 K, and ± 1 K at 270–340 K, with a noise-equivalent temperature difference $(\mathrm{NE}\Delta\mathrm{T}) = 0.3$ K at 300 K [1], [2].

The ASTER project provides the user community with standard products of surface temperature (AST-08) and emissivity (AST-05) using the temperature and emissivity separation (TES) algorithm [3] and the land-leaving TIR radiance product (AST-09T), which is obtained after atmospheric correction of the at-sensor registered radiance [4]. Despite that the TES algorithm provides accurate results in global conditions (± 1.5 K and ± 0.015 emissivity units), some inaccuracies have been found in areas of low spectral contrast due to problems related with scaling errors in emissivity, which can be also increased due to calibration problems and inaccuracies on the atmospheric compensation. This letter presents the results obtained with previously published methods for land-surface temperature (LST) retrieval from TIR data, as two-channel (TC) algorithms. They have been modified or adapted to ASTER characteristics and compared to TES products using ASTER imagery acquired over the agricultural area of Barrax (Albacete, Spain).

II. Theory

Methods for LST from TIR data are based on the radiative-transfer equation, which is given in its simplified form as

$$L_i = \left[\varepsilon_i B_i(T_s) + (1-\varepsilon_i)S_i^{\downarrow}\right]\tau_i + S_i^{\uparrow} \tag{1}$$

where L_i is at-sensor registered radiance at band i, B is the blackbody radiance, T_s is the surface temperature, ε is the surface emissivity, τ is the atmospheric transmissivity, $S^{\downarrow}$ is the downwelling atmospheric irradiance normalized by πsr, and $S^{\uparrow}$ is the upwelling atmospheric-path radiance.

TC algorithms, also called split-window (SW) when working in the spectral range 10–12 μm, are based on the concept of the differential absorption to estimate the atmospheric contribution to the signal. Different algorithms have been published to obtain surface temperature over sea and over land. A review of these methods can be found, for example, in [5]. TC algorithms were developed for ASTER TIR data in [6], but they were focused only on the sea-surface temperature estimation. In this letter, the following TC algorithm for LST retrieval has been considered [7]:

$$\begin{aligned} T_s = {} & T_i + a_1(T_i - T_j) + a_2(T_i - T_j)^2 + a_0 \\ & + (a_3 + a_4 W)(1-\varepsilon) + (a_5 + a_6 W)\Delta\varepsilon \end{aligned} \tag{2}$$

Manuscript received March 22, 2006; revised August 30, 2006. This work was supported in part by the European Union (EAGLE, Project SST3-CT-2003-502057), in part by the Ministerio de Ciencia y Tecnología (DATASAT, Project ESP2005-07724-C05-04), and in part by the European Space Agency (SPARC, Project 18307/04/NL/FF).

The authors are with the Department of Earth, Physics, and Thermodynamics, University of Valencia, Burjassot, 46100 Valencia, Spain.

Digital Object Identifier 10.1109/LGRS.2006.885869

where T_i and T_j are the at-sensor brightness temperatures for the two channels i and j considered (in Kelvin), ε is the mean emissivity, $\varepsilon = 0.5(\varepsilon_i + \varepsilon_j)$, $\Delta\varepsilon$ is the emissivity difference, $\Delta\varepsilon = (\varepsilon_i - \varepsilon_j)$, and W is the atmospheric water-vapor content (in grams per square centimeter). Equation (2) can be obtined by applying (1) to two different TIR channels i and j, as is presented in [8]. Equation (2) may be also simplified, if the emissivity dependence is neglected

$$T_s = T_i + a_1(T_i - T_j) + a_2(T_i - T_j)^2 + a_0 \tag{3}$$

which reproduces the global quadratic algorithm (QUAD) presented in [9].

Other methods that rely on the differential-absorption concept use simply a linear combination of N TIR channels, as is also pointed out in [9]

$$T_s = a_0 + \sum_{i}^{N} a_i T_i. \tag{4}$$

The coefficients involved in (2)–(4) are obtained from simulated data, as is explained in Section III. Hereinafter, the TC algorithms given by (2)–(4) will be refered as $\mathrm{TC}_{\varepsilon-W}$, $\mathrm{TC}_{\mathrm{QUAD}}$, and $\mathrm{TC}_{\mathrm{LIN}}$, respectively.

III. Methodology

A. Simulated Data

The atmospheric parameters (τ, $S_{\downarrow}$, and $S^{\uparrow}$) have been simulated using the radiative-transfer code MODTRAN-4 [10] with the appropriate ASTER system-response functions for the TIR bands for 1761 atmospheric profiles. These atmospheric profiles represent a worldwide set of atmospheric situations, with W values ranging from 0–8 g/cm^2 and air-temperature values in the first layer of atmosphere ranging from 231–312 K [9], [11].

Once the atmospheric parameters are obtained for each ASTER TIR band, at-sensor brightness temperatures (T_i) are simulated from (1) and by inversion of the Planck's law. In (1), T_s was chosen as $T_0 - 5$ K, T_0, $T_0 + 5$ K, $T_0 + 10$ K, and $T_0 + 20$ K, where T_0 is the temperature at the first layer of the atmospheric profiles. The surface emissivities also needed in (1) were extracted from the ASTER spectral library (ASTERlib) [12]. For this purpose, 108 emissivity spectra for natural samples were selected, which include soils, vegetation, water, ice, and those rocks samples with sizes representative at remote-sensing scales (following the ASTERlib notation, rocks with particle size labeled as "whole rock chips"). In this way, a total amount of 950 940 $(1761 \times 5 \times 108)$ simulated data were used to obtain the algorithms coefficients from linear-regression analysis. Another independent simulated database was created in order to test the TC algorithms. For this purpose, the six standard atmospheres included in the MODTRAN code were used, with a scaling factor for the water-vapor content ranging from 0.5 to 1.5 with an increment of 0.1, leading to $6 \times 11 = 66$ atmospheric profiles. As in the previous case, five different values of T_s and 108 emissivity spectra were again considered, leading to a total amount of 35 640 $(66 \times 5 \times 108)$ simulated data. The results of the algorithm coefficients and the test are presented in Section IV.

B. ASTER Imagery and Study Area

The TC algorithms presented in this letter were applied to six ASTER images acquired over the agricultural area of Barrax (Albacete, Spain, 39°3′ N, 2°6′ W, 700 m) on June 28, 2000, August 15, 2000, August 31, 2000, April 28, 2001, August 2, 2001, and July 18, 2004. The whole ASTER images covers an area of 60×60 km^2 (830×700 TIR pixels), whereas the study area has an approximate size of 3×3 km^2 (35×35 TIR pixels). More details regarding the Barrax test site and the ASTER images used can be found in [13] and [14]. The ASTER imagery used in this letter includes Level 1B data (registered radiance at sensor plus geometric correction) and Level 2 standard products AST-08 and AST-05, which refer to the LST and surface emissivities, respectively, obtained with the TES algorithm.

IV. Results and Discussion

A. Algorithms Coefficients and Sensitivity Analysis

Table I shows the values for the TC algorithm coefficients as well as the correlation coefficient (r) and the standard error of estimation (σ) for the different ASTER TIR-band combinations. Table I also shows the errors due to the $\mathrm{NE}\Delta\mathrm{T}$ (0.3 K); the uncertainty on the emissivity (assumed to be 0.02 for ASTER bands 10, 11, and 12, located within 8–9.5 μm, and 0.01 for bands 13 and 14, located within 10–12 μm) and the uncertainty on the W (0.5 g/cm^2). The total error is then obtained by root-sum square of uncertainties, in which the standard error of the estimation σ is also included. A detailed explanation of the sensitivity analysis can be found in [15]. As is expected, the $\mathrm{TC}_{\varepsilon-W}$ algorithm shows a higher r and a lower σ than the $\mathrm{TC}_{\mathrm{QUAD}}$, since it takes into account the dependence on ε and W. However, not all the band combinations provide good results. For example, a classical split-window algorithm using bands 13 and 14 provides errors of 4 K according to the simulated data. These results could be explained by bands 13 and 14 being too close in wavelength, which leads to a high sensitivity to uncertainties due to noise $(e_{\mathrm{NE}\Delta\mathrm{T}} = 2$ K) and emissivity $(e_\varepsilon = 4$ K). Despite these high errors due to the different uncertainties, $\mathrm{TC}_{\varepsilon-W}$ 13 and 14 provides a good statistical fit, with the lowest σ (0.6 K) and high correlation $(r = 0.96)$. From a statistical point of view, $\mathrm{TC}_{\varepsilon-W}$ 10–11 and 10–12 also provide good results, with σ lower than 0.8 K and $r = 0.98$. Combinations involving two consecutive bands provide the highest sensitivity to errors due to emissivity and $\mathrm{NE}\Delta\mathrm{T}$, since consecutive bands are too close in wavelength, excepted for the $\mathrm{TC}_{\varepsilon-W}$ 12 and 13. Combinations between nonconsecutive bands located in the region 8–9.5 μm or combinations between one band located in 8–9.5 μm and another band located in 10–12 μm region provide the best results, with errors below 2 K. In all the cases, the main source of error is due to the uncertainty on the surface emissivity, which highlights the importance of a good estimation of this parameter.

TABLE I
COEFFICIENTS AND ERRORS (IN KELVIN) FOR THE TC ALGORITHMS: $TC_{\varepsilon-W}$ (2), TC_{QUAD} (3) AND TC_{LIN} (4). THE CORRELATION COEFFICIENT(r) AND THE STANDARD ERROR OF ESTIMATION (σ, IN KELVIN) ARE ALSO GIVEN. ERRORS REFER TO THE UNCERTAINTY DUE TO THE NOISE-EQUIVALENT DELTA TEMPERATURE ($e_{NE\Delta T}$) AND TO THE UNCERTAINTIES ON EMISSIVITY (e_ε) AND WATER VAPOR (e_w). THE TOTAL ERROR (e_{total}) IS OBTAINED BY ROOT SUM SQUARE OF UNCERTAINTIES

Algorithm and Bands	a_0	a_1	a_2	a_3	a_4	a_5	a_6	r	σ	$e_{NE\Delta T}$	e_ε	e_w	e_{total}
$TC_{\varepsilon-W}$ 10-11	0.7495	-3.3293	0.0860	48.43	-1.02	101.48	-10.09	0.98	0.7	1.3	3	0.1	3
$TC_{\varepsilon-W}$ 10-12	0.4502	-2.0028	0.0399	52.56	-1.61	58.04	-4.47	0.98	0.8	0.7	1.7	0.1	2
$TC_{\varepsilon-W}$ 10-13	-0.3041	-1.5831	0.0212	44.86	12.26	48.94	2.41	0.93	1.4	0.6	1.3	0.3	2
$TC_{\varepsilon-W}$ 10-14	0.0221	-1.6373	0.0044	32.15	26.14	41.08	8.37	0.89	1.8	0.5	1.4	0.5	2
$TC_{\varepsilon-W}$ 11-12	0.2263	-3.7480	0.0386	55.67	-1.76	147.27	-13.97	0.96	1	1.4	4	0.2	4
$TC_{\varepsilon-W}$ 11-13	0.2492	-1.6496	-0.0004	27.64	24.69	39.15	10.11	0.86	1.7	0.5	1.3	0.4	2
$TC_{\varepsilon-W}$ 11-14	1.9207	-0.6246	0.0537	3.14	41.51	5.29	19.41	0.80	2	0.3	1.1	0.6	2
$TC_{\varepsilon-W}$ 12-13	2.2479	0.0390	0.0496	13.59	30.61	-19.47	18.62	0.86	1.7	0.3	0.8	0.4	1.9
$TC_{\varepsilon-W}$ 12-14	2.7340	0.6678	0.0593	10.83	27.45	-42.96	16.46	0.88	1.6	0.5	0.9	0.3	1.9
$TC_{\varepsilon-W}$ 13-14	0.2665	4.8257	0.5816	35.01	1.33	-282.25	33.77	0.96	0.6	2	4	0.1	4
TC_{QUAD} 10-11	3.4826	-1.1109	0.6547	-	-	-	-	0.78	2	0.9	-	-	3
TC_{QUAD} 10-12	3.5610	-0.5615	0.2548	-	-	-	-	0.74	3	0.5	-	-	3
TC_{QUAD} 10-13	0.6441	-1.5477	0.0136	-	-	-	-	0.88	1.9	0.5	-	-	1.9
TC_{QUAD} 10-14	0.7622	-1.7205	-0.0225	-	-	-	-	0.80	2	0.5	-	-	2
TC_{QUAD} 11-12	4.0866	-0.0713	0.4400	-	-	-	-	0.48	3	0.5	-	-	3
TC_{QUAD} 11-13	1.1340	-1.6575	-0.0339	-	-	-	-	0.76	2	0.5	-	-	2
TC_{QUAD} 11-14	2.7425	-0.6629	0.0544	-	-	-	-	0.65	3	0.3	-	-	3
TC_{QUAD} 12-13	2.5432	-0.7188	0.0451	-	-	-	-	0.74	2	0.3	-	-	2
TC_{QUAD} 12-14	3.3828	-0.0860	0.0927	-	-	-	-	0.73	2	0.3	-	-	2
TC_{QUAD} 13-14	1.7454	0.5433	2.6631	-	-	-	-	0.81	1.4	1.2	-	-	1.8
TC_{LIN} 10 to 14	-7.275	-0.258	0.650	-0.8391	5.0796	-3.6027	-	0.997	1.4	1.9	-	-	2

The TC_{QUAD} and TC_{LIN} algorithms provide higher errors of estimation and lower correlation than $TC_{\varepsilon-W}$, but the total error is similar or even lower. This is due to that these algorithms do not account for the surface emissivity, so the uncertainty of this parameter is not taken into account either. This fact is clearly shown in the combination 13 and 14, with a total error of 4 K for the $TC_{\varepsilon-W}$ and 1.8 K for the TC_{QUAD}. The similar or better results obtained with the TC_{QUAD} algorithms can be also explained taking into account that the major part of the spectra included in the ASTERlib has a low spectral contrast or high-emissivity values, which minimizes the emissivity effect. However, over surfaces with high spectral variations and low-emissivity values, the $TC_{\varepsilon-W}$ is expected to provide clearly better results than TC_{QUAD}, as will be shown in Section IV-C.

B. Algorithms Testing From Independent Simulated Data

The TC algorithms have been tested from an independent simulated database, as explained in Section III-A. The results of the test are shown in Table II. In this case, the $TC_{\varepsilon-W}$ algorithms provide better root-mean-square-error (rmse) values than the TC_{QUAD}, which shows the improvement achieved when the dependence on the surface emissivity is included. The best results are obtained for $TC_{\varepsilon-W}$ 10–11, 10–12, 11–12 (rmse < 1.6 K), and especially for 13 and 14, with an rmse < 1 K. Despite this last combination provided, a high error on the sensitivity analysis (Section IV), in this case, the error on the emissivity or the error due to the $NE\Delta T$ does not have a significant contribution, since simulated data has been used.

C. Intercomparison Between Algorithms and TES Product

The difference between the LST obtained using the TC algorithms presented in Table I and the LST included in the AST-08 has been computed for the six ASTER images acquired over the Barrax site (described in Section III-B) and over the study area of 35 $\times$ 35 TIR. This reduced area has been only considered, because it just covers the experimental agricultural area of Barrax and, also, to avoid cloudy pixels or nonnatural areas as roads or towns. The W values needed to apply $TC_{\varepsilon-W}$ algorithms were approximately estimated from atmospheric soundings launched over sites located around 200 km far from the study area, since errors due to the W uncertainty are typically lower than 0.5 K (see Table I).

Statistical parameters such as bias, standard deviation, and rmse were calculated for the difference between the two LST estimations. The results obtained for the bias and rmse are shown in Fig. 1.

TABLE II
VALUES OF BIAS, STANDARD DEVIATION(σ), AND RMSE OBTAINED IN THE ALGORITHMS TESTING USING INDEPENDENT SIMULATED DATA

	BIAS (K)		σ (K)		RMSE (K)	
Bands	$TC_{\varepsilon-W}$	TC_{QUAD}	$TC_{\varepsilon-W}$	TC_{QUAD}	$TC_{\varepsilon-W}$	TC_{QUAD}
10-11	-0.5	-1	0.9	3	1.0	3
10-12	-0.7	-1	1.0	3	1.2	3
10-13	0	-1	2	3	2	3
10-14	-1	-1	3	4	3	4
11-12	-1.0	-2	1.3	3	1.6	4
11-13	-1	-1	3	3	3	4
11-14	-1	-2	3	4	3	4
12-13	-1	-2	2	3	3	4
12-14	-1.1	-2	1.9	3	2	3
13-14	-0.3	-0.7	0.7	1.5	0.7	1.7

TC_{LIN} algorithm: Bias=-0.2 K, σ=1.8 K and RMSE=1.8 K.

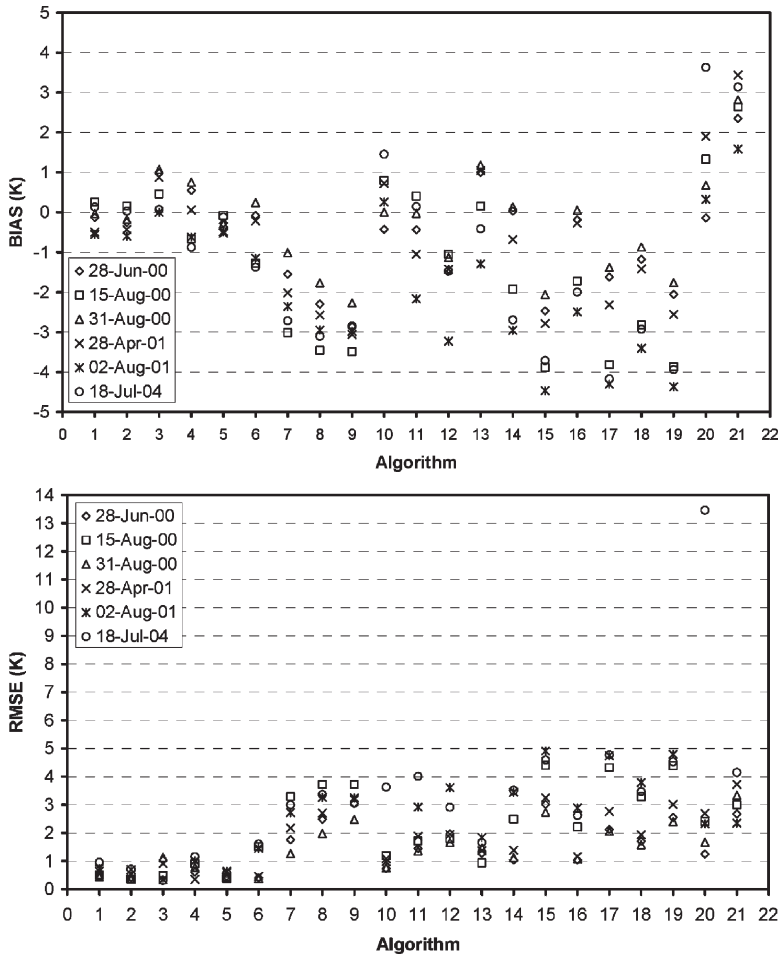

Fig. 1. Bias and rmse obtained for the difference between the LST retrieved using the TC algorithms presented in Table I and the LST provided in the ASTER Standard Product AST-08. In the X axis, band combinations are labeled following the order shown in Table I.

The best results were obtained for $\mathrm{TC}_{\varepsilon-W}$ algorithms and bands combinations from 10–11 to 11–13, with rmse values typically lower than 1 K. The rmse values for the $\mathrm{TC}_{\mathrm{QUAD}}$ and $\mathrm{TC}_{\mathrm{LIN}}$ are within 1–4 K for most cases, which shows a worse performance of these kind of algorithms for LST retrieval, at least in comparison with the TES estimations. An extremely poor result was obtained for the $\mathrm{TC}_{\mathrm{QUAD}}$ 13 and 14 (algorithm no. 20 in Fig. 1) and for the ASTER image acquired on July 18, 2004, with an rmse value higher than 13 K. This strange result was carefully investigated, and finally, an explanation was found by inspection of the AST-05 (TES emissivities) product. Throughout this image (area resized to 35 $\times$ 35 TIR pixels), a few pixels have been found with extremely high spectral contrast (MMD), specifically, more than 1% of the pixels have MMD > 0.2, and some of these pixels show a high decrease between emissivities at bands 13 and 14 (for example, a pixel with MMD $= 0.33$ and a decrease on emissivity between bands 13 and 14 $\Delta\varepsilon = 0.18$ was identified). It should be noted that over agricultural areas, pixels with low MMD are expected. In fact, more than 50% of the pixels for the considered image have MMD < 0.03 (which is the threshold assumed by the TES algorithm to classify the pixel as greybody), and more than 96% of the pixels have MMD < 0.1. This strange result for the emissivity spectrum could be due to a failure of the TES algorithm or to the spectral behavior of the surface itself, despite that this last option seems not to be very probable over an agricultural area. However, it is sure that TC algorithms, which not take into account the surface emissivity ($\mathrm{TC}_{\mathrm{QUAD}}$), can lead to unacceptable inaccuracies over pixels with strong variations on emissivity between bands, especially for bands combination 13 and 14, which are too close in wavelength. In fact, over these "anomalous" pixels, only $\mathrm{TC}_{\varepsilon-W}$ 10–13, 10–14, 11–13, and 11–14 provided acceptable results.

D. Algorithms Testing Using Ground-Truth Data

LST was measured *in situ* in coincidence with the ASTER image acquired on July 18, 2004. Field measurements were carried out in the framework of the SPECTRA Barrax Campaign over five test plots: green grass, alfalfa, bare soil, and two plots of corn. A detailed description of the measurement procedure and previous results for the TES algorithm are presented in [13]. Then, the LST retrieved using the different TC algorithms presented in Table I was compared with the measured LST. The results for the bias, standard deviation, and rmse are shown in Table III. $\mathrm{TC}_{\varepsilon-W}$ provided better results than $\mathrm{TC}_{\mathrm{QUAD}}$, with rmse errors around 1.5 K, except for bands combinations

TABLE III
VALUES OF BIAS, STANDARD DEVIATION (σ), AND RMSE OBTAINED IN THE COMPARISON BETWEEN THE LST RETRIEVED USING THE ALGORITHMS PRESENTED IN TABLE I AND THE LST MEASURED *IN SITU* OVER FIVE DIFFERENT CROPS FOR THE ASTER IMAGE ACQUIRED ON JULY18, 2004

	BIAS (K)		σ (K)		RMSE (K)	
Bands	$TC_{\varepsilon\text{-}W}$	TC_{QUAD}	$TC_{\varepsilon\text{-}W}$	TC_{QUAD}	$TC_{\varepsilon\text{-}W}$	TC_{QUAD}
10-11	-0.6	-0.7	1.3	1.6	1.5	1.8
10-12	-0.6	-1.7	1.3	1.6	1.4	2
10-13	-0.5	-1	1.4	2	1.5	2
10-14	-1.2	-2	1.9	3	2	4
11-12	-0.6	-3	1.6	4	1.7	5
11-13	-2	-2	2	3	3	3
11-14	-3	-3	3	4	4	5
12-13	-3	-3	3	3	4	4
12-14	-3	-3	3	4	4	5
13-14	-0.1	0.6	1.0	1.5	1	1.6

TC_{LIN} algorithm: Bias=1.8 K, σ=1.4 K and RMSE=2 K.

11–13, 11–14, 12–13, and 12–14. TC_{QUAD} 10–11, TC_{QUAD} 13–14 and TC_{LIN} also provided acceptable results with rmse $<$ 2 K, which could be explained due to the high-emissivity values and low spectral contrast of the test plots considered in the comparison. The test of the TES algorithm (AST-08) presented in [13] provided a rmse $= 1.4$ K, which shows that TC algorithms could be also used to extract LST with similar accuracies than the TES algorithm, at least over agricultural areas or surfaces with low spectral contrast and high emissivities.

It should be noted that the comparison shown in this section does not pretend to be a validation of the TC algorithms, since, unfortunately, only one image in coincidence with ground-based measurements is available, but it complements the results presented in the previous sections.

V. CONCLUSION

The TC algorithms provide an alternative to the TES algorithm for retrieving LST from ASTER TIR bands, at least over surfaces with low spectral contrast or high-emissivity values, such as agricultural areas. The main advantage of these algorithms is that the atmospheric correction is included in the algorithm itself. However, it should be noted that the $TC_{\varepsilon-W}$ algorithms require *a priori* knowledge of the surface emissivities, whereas the TES algorithm retrieves both surface emissivities and temperature. A simple approximation for emissivity retrieval using normalized difference vegetation index values can be used as input data to the $TC_{\varepsilon-W}$, as is exposed in [14]. Alternatively, TC_{QUAD} or TC_{LIN} could be also used, since these algorithms do not require *a priori* knowledge of surface emissivities, but they provide worse results than $TC_{\varepsilon-W}$ especially over areas with high spectral contrast and low-emissivity values. It should be noted that TC algorithms applied to ASTER TIR bands provides worse results than other "typical" split-window algorithms applied to bands located within 10–12 μm, since ASTER bands 13 and 14 are too close in wavelength, which leads to a high sensitivity of the algorithm to errors on emissivity and also to the $\mathrm{NE}\Delta\mathrm{T}$.

The authors plan to investigate in the future the feasibility of using TC algorithms as a first guess for the LST and improve the TES estimations.

ACKNOWLEDGMENT

The authors would like to thank A. Gillespie, D. Sabol, and W. T. Gustafson (University of Washington) for their helpful scientific and technical support.

REFERENCES

[1] Y. Yamaguchi, A. B. Kahle, H. Tsu, T. Kawakami, and M. Pniel, "Overview of Advanced Spaceborne Thermal Emission and Reflection Radiometer (ASTER)," *IEEE Trans. Geosci. Remote Sens.*, vol. 36, no. 4, pp. 1062–1071, Jul. 1998.

[2] M. Abrams, "The Advanced Spaceborne Thermal Emission and Reflection Radiometer (ASTER): Data products for the high spatial resolution imager on NASA's Terra platform," *Int. J. Remote Sens.*, vol. 21, no. 5, pp. 847–859, 2000.

[3] A. Gillespie, S. Rokugawa, T. Matsunaga, J. S. Cothern, S. Hook, and A. B. Kahle, "A temperature and emissivity separation algorithm for Advanced Spaceborne Thermal Emission and Reflection Radiometer (ASTER) images," *IEEE Trans. Geosci. Remote Sens.*, vol. 36, no. 4, pp. 1113–1126, Jul. 1998.

[4] F. Palluconi, G. Hoover, R. Alley, M. Jentoft-Nilsen, and T. Thompson, "An atmospheric correction method for ASTER thermal radiometry over land," in "Algorithm Theoretical Basis Document," Jet Propulsion Lab., Pasadena, CA, 1999.

[5] Y. H. Kerr, J. P. Lagouarde, F. Nerry, and C. Ottlé, "Land surface temperature retrieval techniques and applications: Case of the AVHRR," in *Thermal Remote Sensing in Land Surface Processes*, D. A. Quattrochi and J. C. Luvall, Eds. Boca Raton, FL: CRC, 2004, pp. 33–109.

[6] K. Arai, "Sea surface temperature (SST) estimation accuracy assessment for ASTER/TIR—An effectiveness of 8.3 μm of water vapour absorption band for SST retrieval," *Can. J. Remote Sens.*, vol. 26, no. 6, pp. 576–579, 2000.

[7] J. A. Sobrino and N. Raissouni, "Toward remote sensing methods for land cover dynamic monitoring: Application to Morocco," *Int. J. Remote Sens.*, vol. 21, no. 2, pp. 353–366, 2000.

[8] J. A. Sobrino, Z.-L. Li, M. P. Stoll, and F. Becker, "Multi-channel and multi-angle algorithms for estimating sea and land surface temperature with ATSR data," *Int. J. Remote Sens.*, vol. 17, no. 11, pp. 2089–2114, 1996.

[9] C. François and C. Ottlé, "Atmospheric corrections in the thermal infrared: Global and water vapor dependent split-window algorithms-applications to ATSR and AVHRR data," *IEEE Trans. Geosci. Remote Sens.*, vol. 34, no. 2, pp. 457–470, Mar. 1996.

[10] A. Beck, G. P. Anderson, P. K. Acharya, J. H. Chetwynd, L. S. Bernstein, E. P. Shettle, M. W. Matthew, and S. M. Adler-Golden, *MODTRAN4 User's Manual*. Hanscom AFB, MA: Air Force Res. Lab., 1999.

[11] Z.-L. Li, L. Jia, Z. Su, Z. Wan, and R. Zhang, "A new approach for retrieving precipitable water from ATSR2 split-window channel data over land area," *Int. J. Remote Sens.*, vol. 24, no. 24, pp. 5095–5117, 2003.

[12] S. J. Hook, *The ASTER Spectral Library*, Pasadena, CA: Jet Propulsion Lab., 1999. [Online]. Available: http://speclib.jpl.nasa.gov

[13] J. A. Sobrino, J. C. Jiménez-Muñoz, L. Balick, A. Gillespie, D. Sabol, and W. T. Gustafson, "Accuracy of ASTER level-2 thermal-infrared standard products of an agricultural area in Spain," *Remote Sens. Environ.* to be published. DOI: 10.1016/j.rse.2006.08.010.

[14] J. C. Jiménez-Muñoz, J. A. Sobrino, A. Gillespie, D. Sabol, and W. T. Gustafson, "Improved land surface emissivities over agricultural areas using ASTER NDVI," *Remote Sens. Environ.*, vol. 103, no. 4, pp. 474–487, 2006.

[15] J. A. Sobrino, J. C. Jiménez-Muñoz, J. El-Kharraz, M. Gómez, M. Romaguera, and G. Sòria, "Single-channel and two-channel methods for land surface temperature retrieval from DAIS data and its application to the Barrax site," *Int. J. Remote Sens.*, vol. 25, no. 1, pp. 215–230, 2004.